RSC Advances

PAPER

View Article Online
View Journal | View Issue

Cite this: *RSC Adv.*, 2024, **14**, 11728

Organic dye-loaded reduced titanium dioxide as a broadband saturable absorber for ultrafast fiber lasers

Xiaochan Lu,†[ac] Shuang Li,†[a] Miao Yan,[b] Jianming Chen,[a] Tingting Deng,[a] Guohui Nie,[a] Zhenhong Wang,[a] Hu Liang*[b] and Bin Zhang *[a]

Received 29th December 2023
Accepted 1st April 2024

DOI: 10.1039/d3ra08925h

rsc.li/rsc-advances

As a rising star among metal oxide nanomaterials, titanium dioxide (TiO_2) has been widely investigated and employed in optical applications because of its excellent optical properties. In this work, we demonstrate the efficient and broadband nonlinear photonic properties of methylene blue (MB)-loaded reduced TiO_2 (TiO_{2-x}-MB) and explore the performance of a TiO_{2-x}-MB-microfiber photonic device in broadband ultrafast photonics. Within an erbium-doped fiber laser (EDFL) system, utilizing the TiO_{2-x}-MB-microfiber photonic device as a saturable absorber (SA), steady mode-locked pulses together with chaotic pulses were successfully achieved at the wavelength of 1.55 μm. Furthermore, by incorporating the TiO_{2-x}-MB SA into a thulium-doped fiber laser (TDFL) system, an ultrashort single pulse and multiple pulses were obtained at 2.0 μm. These results indicate that TiO_{2-x}-MB is an excellent nanomaterial for use in mode-locked lasers, being an alternative candidate for ultrafast fiber lasers *via* exploiting the chemical and physical properties of oxide nanomaterials.

1 Introduction

Ultrafast fiber lasers are widely used in various military and civilian applications,[1–3] such as optical communication[4] and precision machining.[5,6] One of the main methods for generating ultrashort pulses is passive mode-locked technology, where the key is to introduce a saturable absorber (SA) into the laser cavity. Mode-locked fiber lasers can be realized using suitable materials as SAs, providing advantages in performance and output stability.[6] Existing saturable absorber materials include semiconductor saturable absorber mirrors[7,8] and two-dimensional materials represented by graphene,[9,10] molybdenum disulfide (MoS_2)[11,12] and black phosphorus.[13,14] In addition, various materials have been used for mode-locked devices in ultrafast lasers, including $SnSe_2$,[15] $GeAs_2$,[16] rGO-Co_3O_4 (ref. 17) and WCNs.[18] However, the investigation of new materials for use as SAs is still in early stages. Therefore, it is necessary to explore novel materials as alternative SAs with excellent nonlinear optical properties for achieving mode-locked ultrashort pulse lasers.

Recently, titanium dioxide (TiO_2) nanomaterials have been attracting increasing research interest because of their excellent photocatalytic properties, good biocompatibility and excellent chemical stability. Their potential application in all-optical switching devices has also received extensive attention, especially in thin film form.[19] TiO_2 sheets have strong planar bonding and weak van der Waals coupling, making them suitable for mechanical or chemical exfoliation. In 2015, Ahmad *et al.* obtained Q-switched pulses in an EDFL with TiO_2 film as the SA.[20] Afterwards, Reddy *et al.* demonstrated a passively mode-locked thulium-holmium-doped fiber laser based on a TiO_2 SA and observed the ultrashort pulses.[21] Further, TiO_2-doped fiber (TiO_2 DF) was utilized as a passive SA in an EDFL,[22] providing a stable and self-powered mode-locked pulse laser under proper conditions. Thus, it is important to continue the research on ultrafast fiber lasers with TiO_2 SAs in the 1.55 μm and 2.0 μm region, which is of great significance, due to the great potential in various fields, including supercontinuum generation[23] and material processing.[24]

In this work, TiO_2 was reduced into TiO_2 nanoparticles (TiO_{2-x}), which have a low band gap compared with undoped TiO_2 particles. In addition, the organic dye methylene blue (MB) was used as a dopant to modify TiO_{2-x} to form the TiO_{2-x}-MB nanostructure, which further enhanced its working wavelength. Then, we fabricated the TiO_{2-x}-MB nanomaterial by utilizing a liquid-phase exfoliation process. Furthermore, a TiO_{2-x}-MB photonic device was constructed on microfiber *via* an optical deposition method, and the nonlinear optical absorption properties at 1.55 μm and 2 μm were evaluated. We then studied the

[a]*Institute of Microscale Optoelectronics and Translational Medicine, School of Pharmaceutical Sciences, Department of Otolaryngology, The First Affiliated Hospital (Shenzhen Second People's Hospital), Health Science Center, Shenzhen University, Shenzhen 518035, China. E-mail: binzhang@email.szu.edu.cn*

[b]*Tianjin Navigation Instruments Research Institute, Tianjin 300131, China. E-mail: ymirlh@163.com*

[c]*Department of Otorhinolaryngology, Peking University Shenzhen Hospital, Shenzhen, 518036, China*

† These authors contributed equally to this work.

performance of the TiO_{2-x}-MB photonic device as a SA in EDFL and TDFL systems. Based on the outstanding saturable absorption of the TiO_{2-x}-MB photonic device, we realized mode-locked pulses together with chaotic pulses in the EDFL. In addition, we obtained stable single pulses as well as multiple pulses in the TDFL using the TiO_{2-x}-MB photonic device as the SA. Multi-pulse operation in a TDFL with TiO_{2-x}-MB SA is reported for the first time. Our experimental results suggest that the TiO_{2-x}-MB photonic device is suitable for efficient application in ultrafast photonics. Besides, this work will promote the exploration of the optical behavior of metal oxides and further applications of optimized nanomaterials in ultrafast fiber lasers.

2 Material preparation and characterization

2.1 Preparation and characterization of the TiO_{2-x}-MB nanomaterial

The TiO_{2-x}-MB nanomaterial was obtained *via* the introduction of Ti^{3+} ions on the surface of TiO_2 by reducing TiO_2 particles followed by modification with the organic dye MB.[25,26] Briefly, 6 g of sodium borohydride was added to 60 mL of water, then 0.50 g of anatase TiO_2 powder was added, and the hydrothermal reaction was carried out in an autoclave at 180 °C for 16 hours. Subsequently, the reaction solution was centrifuged (10 000 rpm) for 5 minutes, and the centrifuged TiO_{2-x} powder doped with Ti^{3+} was alternately rinsed using deionized water and ethanol three times, with the TiO_{2-x} powder and washing solution being separated by centrifugation each time. The TiO_{2-x} powder was collected and further dried in air at 60 °C for 10 hours. Then, 250 mg of the TiO_{2-x} powder was dispersed in 50 mL of 7×10^{-5} M MB solution (TiO_2 : MB = 250 : 1) and mixed using a magnetic stirrer at room temperature for 60 minutes. Upon reaction, the precipitate and solution were separated by centrifugation. The resulting precipitate was then rinsed with water and acetone three times alternately, then dried at 25 °C for 12 hours and ground to obtain the TiO_{2-x}-MB nanomaterial.

Fig. 1(a) shows the absorption spectra for TiO_2, TiO_{2-x} and TiO_{2-x}-MB, indicating that the prepared TiO_{2-x}-MB material has good absorption in the 500–2000 nm region. The dynamic light scattering (DLS) characterization of TiO_2, TiO_{2-x} and TiO_{2-x}-MB is shown in Fig. 1(b), which was carried out to measure their average particle size. As can be seen from the figure, the average particle size of TiO_{2-x} without MB incorporation is 382 nm, which is close to the average particle size of unmodified TiO_2 (363 nm), indicating that the nanoparticle size was maintained after the reduction of the TiO_2 nanoparticles. The particle size of the prepared TiO_{2-x}-MB is between 400 and 1100 nm, and the average particle size of the main component is 688 nm. The results show that the loading of MB obviously increases the particle size of the material. Scanning electron microscope (SEM) images of TiO_2, TiO_{2-x}, and TiO_{2-x}-MB indicate that the modification of MB on the TiO_{2-x} nanomaterial increases the particle size of the nanoparticles (Fig. 1(c–e)), which is consistent with DLS results. The high-resolution transmission electron microscopy (HRTEM) image of the prepared TiO_{2-x}-MB nanostructure is shown in Fig. 1(f). The lattice stripes with interlayer distance of 0.350 nm can be observed from HRTEM, which corresponds to the (101) crystal surface of TiO_2.

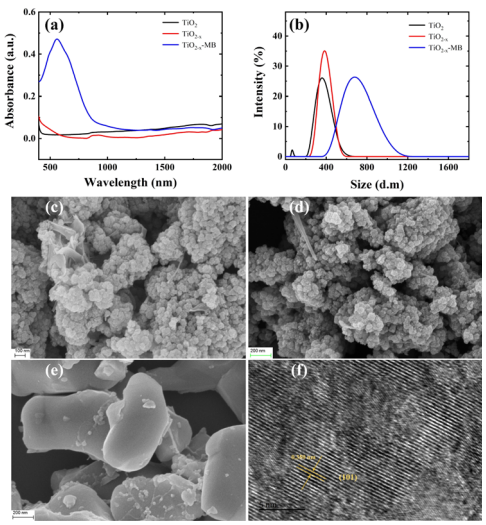

Fig. 1 Characterization of the TiO_{2-x}-MB nanomaterial. (a) Absorption spectra and (b) DLS spectra for TiO_2, TiO_{2-x} and TiO_{2-x}-MB. SEM images of (c) TiO_2, (d) TiO_{2-x}, and (e) TiO_{2-x}-MB. (f) HRTEM image of TiO_{2-x}-MB.

2.2 Nonlinear optical properties of TiO_{2-x}-MB SA

First, the above-prepared TiO_{2-x}-MB nanomaterial was uniformly dispersed in isopropyl alcohol. Then, the TiO_{2-x}-MB nanomaterial was deposited on a microfiber as an optical device using the optical deposition method.[27] Herein, the microfiber is drawn from a standard single-mode fiber using a typical flame-brushing method. The fabricated microfiber has a diameter of approximately 12 μm and exhibits an insertion loss as low as ~0.5 dB at 1550 nm. Because of the long interaction length, a strong evanescent field interaction occurs when the light propagates along the TiO_{2-x}-MB sample, which significantly improves the damage threshold of the TiO_{2-x}-MB SA. Afterwards, the nonlinear transport behavior of the TiO_{2-x}-MB SA at different wavelengths was investigated by utilizing the twin-power-meter method.[28] The input fiber laser sources are a homemade mode-locked EDFL (1565 nm, 98 MHz, 500 fs) and a TDFL (1957 nm, 12 MHz, 1 ps). The TiO_{2-x}-MB SA displays typical nonlinear optical absorption properties, as shown in Fig. 2(a) and (b). The optical modulation depths (ΔT) of the

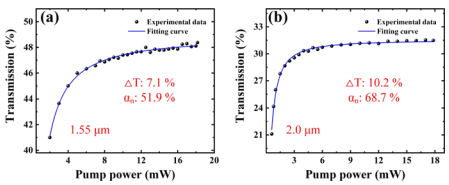

Fig. 2 Nonlinear absorption transmission curves for TiO_{2-x}-MB SA on a microfiber at (a) 1.55 μm and (b) 2 μm.

TiO_{2-x}-MB SAs are 7.1 % at 1.55 μm and 10.2 % at 2.0 μm, respectively, and corresponding non-saturable losses (αn) are 51.9% and 68.7%, respectively. These characteristics indicate that the TiO_{2-x}-MB has typical nonlinear optical absorption and is suitable for application in ultrafast photonics.

3 Ultrafast photonics applications

The fabricated TiO_{2-x}-MB SA can be spliced into the EDFL and TDFL, as depicted in Fig. 3. The pump laser is launched into the gain fiber (3 m long EDF or 2.7 m long TDF) using a wavelength-division multiplexer (WDM). The central wavelengths of pump lasers are ~980 nm for EDFL and ~1570 nm for TDFL. A polarization-independent isolator (PI-ISO) was used to guarantee the unidirectional operation of the fiber laser. For the EDFL, the 30% port of the 3 : 7 optical coupler (OC) is used as the output. For the TDFL, the 20% port of the 2 : 8 OC is applied as the output. The homemade methylene blue (MB)-loaded reduced TiO_2 (TiO_{2-x}-MB) on microfiber is used as the saturable absorber (SA). A polarization controller (PC) with three paddles is used to finely adjust the intracavity polarization state. The total lengths of the EDFL and TDFL are ~19.1 m and ~21.4 m, respectively. The output pulses can be recorded using a commercial optical spectrum analyzer, oscilloscope, radio-frequency (RF) analyzer and autocorrelator.

3.1 Mode-locked pulses and chaotic pulses in the EDFL

Because of the strong nonlinear optical absorption of the TiO_{2-x}-MB SA, it is easy to obtain mode-locked pulses by properly adjusting the pump power and polarization controller (PC). The stable mode-locked pulses at a pump power of 40 mW are shown in Fig. 4. Clearly, the optical spectral center is about 1556.14 nm, and the 3 dB bandwidth is approximately 5.03 nm, as shown in Fig. 4(a). Moreover, typical sidebands are observed on the left and right of the optical spectrum. Besides, an obvious continuous wave (CW) peak can be seen at 1557.34 nm, resulting from the operation state with imperfect mode locking.[11] The pulse trains are illustrated in Fig. 4(b). The temporal separation of the two pulses is ~100.7 ns. Therefore, the corresponding repetition frequency is 9.93 MHz, matching the total cavity length. Fig. 4(c) presents the measured radio-frequency (RF) spectrum. Obviously, the signal-to-noise ratio (SNR) is ~59.8 dB, indicating that the laser operation maintains a relatively steady state. The autocorrelation curve in Fig. 4(d) has a full width at half maximum of ~1.51 ps, corresponding to a pulse duration of ~978 fs if a $sech^2$ fit is assumed. Thus, the time-bandwidth product (TBP) is higher than the transform-limiting of 0.315, indicating that the obtained pulses have a slight chirp.

Further, chaotic-pulse bunches can be observed by suitably enhancing the pump power and adjusting the paddles of the PC due to the energy quantization of the ultrashort pulses under higher pump power.[29] Fig. 5 depicts their output characteristics at 400 mW. The measured optical spectrum shows a center of 1558.84 nm with a 3 dB bandwidth of 0.2 nm, as illustrated in Fig. 5(a). In addition, no obvious sidebands were observed in the optical spectrum. The pulse sequence based on the 1 GHz low-speed oscilloscope is presented in Fig. 5(b). The temporal separation of 100.7 ns indicates that the pulse operation follows the fundamental frequency regime. We also measured temporal pulse trains using a 20 GHz real-time oscilloscope, as shown in Fig. 5(c). Several obvious multiple-pulse bunch envelopes can be seen in the temporal domain. Besides, the intensities of these

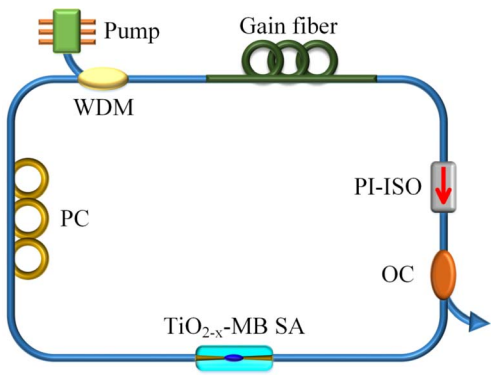

Fig. 3 Schematic diagram of the ultrafast fiber laser setup with the TiO_{2-x}-MB SA.

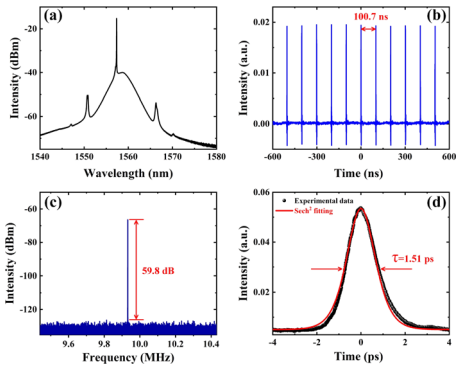

Fig. 4 Mode-locked operation of the EDFL with the TiO_{2-x}-MB SA. (a) Optical spectrum, (b) temporal trains, (c) RF spectrum, and (d) auto-correlation curve.

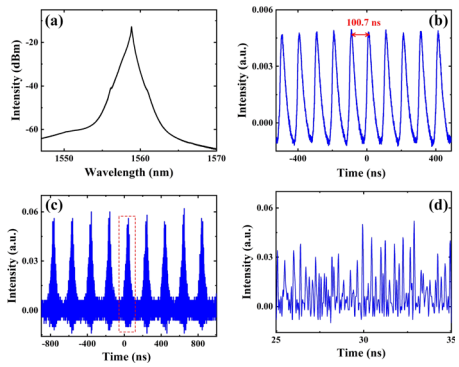

Fig. 5 Chaotic-pulse operation of the EDFL with the TiO_{2-x}-MB SA. (a) Optical spectrum, (b) temporal trains with low-speed oscilloscope, (c) temporal trains with high-speed oscilloscope, and (d) close-up view of the red dotted section in (c).

bunches are chaotic and random. Furthermore, the details of a single envelope are shown in Fig. 5(d). It is obvious that the single multiple-pulse bunch envelope consists of many smaller pulses, where these random pulses have varying intensities with an irregular trend.

3.2 Ultrashort single pulse and multiple pulses in the TDFL

To dig into the nonlinear optical absorption behaviors of the as-fabricated TiO_{2-x}-MB SA, especially the phenomenon when the wavelength is extended to the 2.0 μm region, a TDFL system was constructed, as shown in Fig. 3. By raising the pump power to 240 mW, it appears that the mechanism might be assigned to CW. Through manipulating accessories together with the power, steady mode-locked operation was obtained. Fig. 6 clearly shows the output pulse performance of this system at 300 mW. There are obvious Kelly sidebands located in the spectrum, as displayed in Fig. 6(a). As can be seen, the resulting spectrum is centered at 1888.8 nm, with a full width at half maximum of 2.65 nm. Furthermore, there are noticeable characteristic dips, which should be attributed to the absorption line for water from the atmosphere. Moreover, Fig. 6(b) confirmed that the temporal pulse has a separation of 103.3 ns, suggesting a repetition rate of 9.68 MHz, matching well with the cavity length. The operation steadiness of the laser is demonstrated, with the SNR of the recorded RF spectrum reaching ~60.2 dB (Fig. 6(c)). In addition, to check the data quality of the output pulses, we recorded the autocorrelation trace shown in Fig. 6(d). The measured FWHM is 2.36 ps, which suggests that the pulse width of the autocorrelation curve should be 1.53 ps by assuming a sech² intensity profile. Furthermore, the estimated TBP value is ~0.340, manifesting a slightly chirped pulse. Moreover, the output performance of ultrafast fiber lasers based on various SAs reported in recent years is summarized in Table 1. As can be seen from this table, the TiO_{2-x}-MB material can be used as an excellent broadband SA for obtaining ultrashort pulses in mode-locked fiber lasers.

It is well-known that when the pump power is at a high level, the mode-locked fiber cavity easily generates complicated pulses because of the soliton energy quantization effect.[29] Therefore, when enhancing the pump power continuously, our TDFL operation will exhibit a multiple-pulse state. The output optical spectrum of multiple pulses at 340 mW is displayed in Fig. 7(a). As shown, the spectrum is centered at 1888.63 nm, with a FWHM of 2.25 nm. Besides, Fig. 7(b) shows that the measured pulse signals largely rely on the high-speed oscilloscope. The corresponding details are depicted in Fig. 7(c), indicating that the output pulses are made up of six pulses. The first pulse distance is ~1.37 ns, and the final one is ~1.06 ns. The average pulse distance is about 1.05 ns. Obviously, the pulse distance trend is changeable. Further, optical spectra were studied at four pump powers, with the results presented in Fig. 8(a). Clearly, the spectral shape is almost unchanged, despite the enhanced pump power. The number of pulses in a single bunch of pulses at these pump powers was investigated, as illustrated in Fig. 8(b). With increasing pump power, a nearly linear increase in the number of pulses is observed from 1 to 12. Similar phenomena have been obtained in EDFLs.[39–42] This is the first time that such an operation regime has been observed in a TDFL, to the best of our knowledge. The formation of this special pulse regime is closely associated with the slow recovery

Table 1 Summary of the performance of different materials used as SAs in ultrafast fiber lasers at 1.55 μm and 2.0 μm

Material	Wavelength (nm)	Duration (ps)	Frequency (MHz)	Ref.
NiS_2	1560.2	0.524	21.1	30
Ti_2CT_x	1530.85	0.265	19	31
$SnSe_2$	1560.14	0.598	10.83	15
Graphdiyne	1565.72	0.940	5.05	32
WS_2	1557	1.32	8.86	33
TiO_{2-x}-MB	1556.14	0.978	9.93	This work
WS_2	1941	1.3	34.8	34
Bi_2Te_3	1909.5	1.26	21.5	35
Black phosphorus	1898	1.58	19.2	36
WSe_2	1863.96	1.16	11.36	37
SnSe	1897	2.12	5.98	38
TiO_{2-x}-MB	1888.8	1.53	9.68	This work

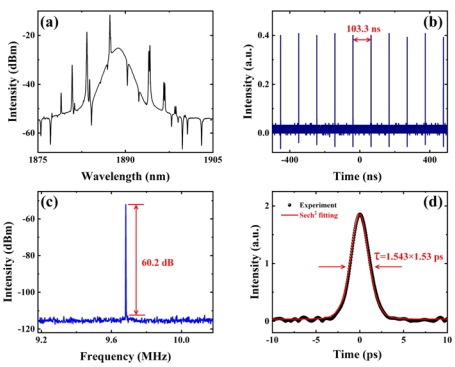

Fig. 6 Single-pulse operation of the TDFL with the TiO_{2-x}-MB SA. (a) Optical spectrum, (b) temporal trains, (c) RF spectrum, and (d) autocorrelation curve.

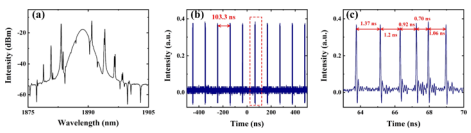

Fig. 7 Multiple-pulse operation of the TDFL with the TiO_{2-x}-MB SA. (a) Optical spectrum, (b) temporal trains with high-speed oscilloscope, and (c) close-up view of the red dotted section in (b).

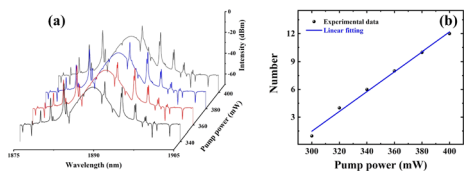

Fig. 8 (a) Optical spectra and (b) pulse numbers with different pump powers.

and depletion mechanism for the gain in the EDFL.[39] When the pump power is elevated one step further, multiple pulses disappear, and the pulse operation becomes unstable, which may be attributed to the strong and weak interactions of these multiple pulses in this state.

4 Conclusions

In summary, this work has reported the fabrication and characterization of a TiO_{2-x}-MB nanomaterial, and its application in nonlinear optics in ultrafast fiber lasers at 1.55 μm and 2.0 μm. Due to the excellent nonlinear optical characteristics of the TiO_{2-x}-MB nanomaterial, a TiO_{2-x}-MB-decorated microfiber device was fabricated and used as a SA. Using the TiO_{2-x}-MB SA in an EDFL, stable mode-locked pulses and chaotic pulses were successfully obtained. Moreover, the TiO_{2-x}-MB SA can be used in a TDFL, generating not only a single pulse but also multiple pulses. Our results suggest that TiO_{2-x}-MB has promising potential for use in ultrafast fiber lasers, extending the application of these metal oxides, which are generally used as photocatalysts and providing efficient candidates for use in nonlinear photonics.

Author contributions

Xiaochan Lu and Shuang Li: conceptualization, investigation, writing – original draft preparation. Miao Yan and Jianming Chen: investigation, formal analysis. Tingting Deng: data curation, methodology. Guohui Nie and Zhenhong Wang: supervision. Hu Liang and Bin Zhang: resources, funding acquisition.

Conflicts of interest

The authors declare that they have no known competing financial interests or personal relationships that could have appeared to influence the work reported in this paper.

Acknowledgements

This work was supported by the National Key Research and Development Project (Grant No. 2022YFA0912500, 2020YFC2005205, and 2020YFC2005200), National Natural Science Foundation of China (Grant No. 52203335, 62005178, 82002936, 62105307, 82192865 and 81970875), Guangdong Basic and Applied Basic Research Foundation (Grant No. 2023A1515010093, 2023A1515220240), Shenzhen Science and Technology Innovation Committee (Grant No. ZDSYS201707281114196, KCXFZ20201221173413038, LCYSSQ20220823091403007, JCYJ20190806163209126, JCYJ20190808143611709, JCYJ20200109105216803, JCYJ20220809170611004 and JCYJ20220530150414031), Sanming Project of Medicine in Shenzhen (Grant No. SZSM202211022), and Development and Reform Commission of Shenzhen Municipality.

Notes and references

1 M. E. Fermann and I. Hartl, *Nat. Photonics*, 2013, **7**, 868–874.
2 J. Ma, Z. Qin, G. Xie, L. Qian and D. Tang, *Appl. Phys. Rev.*, 2019, **6**, 021317.
3 G. Chang and Z. Wei, *iScience*, 2020, **23**, 101101.
4 K. Anbarasi, C. Hemanth and R. G. Sangeetha, *Opt. Laser Technol.*, 2017, **97**, 161–171.
5 Z. Lin and M. Hong, *Ultrafast Sci.*, 2021, **2021**, 9783514.
6 T. Jiang, K. Yin, C. Wang, J. You, H. Ouyang, R. Miao, C. Zhang, K. Wei, H. Li, H. Chen, R. Zhang, X. Zheng, Z. Xu, X. Cheng and H. Zhang, *Photonics Res.*, 2020, **8**, 78–90.
7 L. M. Zhao, D. Y. Tang, X. Wu, H. Zhang and H. Y. Tam, *Opt. Lett.*, 2009, **34**, 3059–3061.
8 Y. Mashiko, E. Fujita and M. Tokurakawa, *Opt. Express*, 2016, **24**, 26515–26520.
9 Q. Bao, H. Zhang, Y. Wang, Z. Ni, Y. Yan, Z. X. Shen, K. P. Loh and D. Y. Tang, *Adv. Funct. Mater.*, 2009, **19**, 3077–3083.
10 M. Pawliszewska, T. Martynkien, A. Przewłoka and J. Sotor, *Opt. Lett.*, 2018, **43**, 38–41.
11 H. Xia, H. Li, C. Lan, C. Li, J. Du, S. Zhang and Y. Liu, *Photonics Res.*, 2015, **3**, A92–A96.
12 Y. Zhang, J. Zhu, P. Li, X. Wang, H. Yu, K. Xiao, C. Li and G. Zhang, *Opt. Commun.*, 2018, **413**, 236–241.
13 M. Zhang, Q. Wu, F. Zhang, L. Chen, X. Jin, Y. Hu, Z. Zheng and H. Zhang, *Adv. Opt. Mater.*, 2019, **7**, 1800224.
14 K. Park, J. Lee, Y. T. Lee, W.-K. Choi, J. H. Lee and Y.-W. Song, *Ann. Phys.*, 2015, **527**, 770–776.
15 Z. Wang, B. Zhang, B. Hu, Z. Li, C. Ma, Y. Chen, Y. Song, H. Zhang, J. Liu and G. Nie, *Photonics Res.*, 2020, **8**, 1687–1696.
16 S. Liu, G. Li, F. Zhu, H. Huang, J. Lu, J. Qu, L. Li and Q. Wen, *Adv. Funct. Mater.*, 2022, **32**, 2112252.
17 M. An, Z. Pan, X. Li, W. Wang, C. Jiang, G. Li, P. Guo, H. Lu, Y. Han, X. Chen and Z. Zhang, *ACS Appl. Mater. Interfaces*, 2022, **14**, 53971–53980.
18 F. Wang, D. Lan, J. Zhao, Y. Qu, X. Zhou, X. Zhang and T. Cheng, *Opt. Laser Technol.*, 2023, **158**, 108778.
19 H. Long, A. Chen, G. Yang, Y. Li and P. Lu, *Thin Solid Films*, 2009, **517**, 5601–5604.
20 H. Ahmad, S. A. Reduan, Z. A. Ali, M. A. Ismail, N. E. Ruslan, C. S. J. Lee, R. Puteh and S. W. Harun, *IEEE Photonics J.*, 2016, **8**, 1500107.
21 P. H. Reddy, M. F. A. Rahman, M. C. Paul, A. A. Latiff, A. H. A. Rosol, S. Das, A. Dhar, S. K. Bhadra, K. Dimyati and S. W. Harun, *Optik*, 2018, **158**, 1327–1333.
22 M. F. Mohd Rusdi, A. A. Latiff, M. C. Paul, S. Das, A. Dhar, H. Ahmad and S. W. Harun, *Opt. Laser Technol.*, 2017, **89**, 16–20.
23 Z. Zheng, D. Ouyang, J. Zhao, M. Liu, S. Ruan, P. Yan and J. Wang, *Photonics Res.*, 2016, **4**, 135–139.
24 I. Mingareev, N. Gehlich, T. Bonhoff, A. Abdulfattah, A. M. Sincore, P. Kadwani, L. Shah and M. Richardson, *Int. J. Adv. Des. Manuf. Technol.*, 2016, **84**, 2567–2578.
25 R. Ren, Z. Wen, S. Cui, Y. Hou, X. Guo and J. Chen, *Sci. Rep.*, 2015, **5**, 10714.
26 E. Savinkina, L. Obolenskaya and G. Kuzmicheva, *Appl. Nanosci.*, 2015, **5**, 125–133.
27 Y. Song, K. You, Y. Chen, J. Zhao, X. Jiang, Y. Ge, Y. Wang, J. Zheng, C. Xing and H. Zhang, *Nanoscale*, 2019, **11**, 12595–12602.

28 Z.-C. Luo, M. Liu, H. Liu, X.-W. Zheng, A.-P. Luo, C.-J. Zhao, H. Zhang, S.-C. Wen and W.-C. Xu, *Opt. Lett.*, 2013, **38**, 5212–5215.
29 D. Y. Tang, L. M. Zhao, B. Zhao and A. Q. Liu, *Phys. Rev. A*, 2005, **72**, 043816.
30 P. Wang, H. Zhang, Y. Yin, Q. Ouyang, Y. Chen, E. Lewis, G. Farrell, M. Tokurakawa, S. Wadi Harun, C. Wang and S. Li, *Opt. Laser Technol.*, 2020, **132**, 106492.
31 Y. Shi, N. Xu and Q. Wen, *J. Lightwave Technol.*, 2020, **38**, 1975–1980.
32 J. Guo, Z. Wang, R. Shi, Y. Zhang, Z. He, L. Gao, R. Wang, Y. Shu, C. Ma, Y. Ge, Y. Song, D. Fan, J. Xu and H. Zhang, *Adv. Opt. Mater.*, 2020, **8**, 2000067.
33 D. Mao, Y. Wang, C. Ma, L. Han, B. Jiang, X. Gan, S. Hua, W. Zhang, T. Mei and J. Zhao, *Sci. Rep.*, 2015, **5**, 7965.
34 M. Jung, J. Lee, J. Park, J. Koo, Y. M. Jhon and J. H. Lee, *Opt. Express*, 2015, **23**, 19996–20006.
35 K. Yin, B. Zhang, L. Li, T. Jiang, X. Zhou and J. Hou, *Photonics Res.*, 2015, **3**, 72–76.
36 H. Yu, X. Zheng, K. Yin, X. a. Cheng and T. Jiang, *Appl. Opt.*, 2015, **54**, 10290–10294.
37 J. Wang, W. Lu, J. Li, H. Chen, Z. Jiang, J. Wang, W. Zhang, M. Zhang, I. L. Li, Z. Xu, W. Liu and P. Yan, *IEEE J. Sel. Top. Quantum Electron.*, 2018, **24**, 1–6.
38 Z. Wang, F. Li, J. Guo, C. Ma, Y. Song, Z. He, J. Liu, Y. Zhang, D. Li and H. Zhang, *Adv. Opt. Mater.*, 2020, **8**, 1902183.
39 A. Zaviyalov, P. Grelu and F. Lederer, *Opt. Lett.*, 2012, **37**, 175–177.
40 Z. Wang, Z. Wang, Y. g. Liu, R. He, G. Wang, G. Yang and S. J. C. O. L. Han, *Chin. Opt. Lett.*, 2017, **15**, 080605.
41 Z. Wang, X. Wang, Y. Song, J. Liu and H. Zhang, *Phys. Rev. A*, 2020, **101**, 013825.
42 Y.-T. Yang, Y. Zou, Q. Zeng, Y.-F. Song, K. Wang and Z.-H. Wang, *Acta Phys. Sin.*, 2022, **71**, 134201–134208.